

Influence of Atmospheric Rivers on Alaskan River Ice

Russ Limber^{1,2}, Elias C. Massoud², Jitendra Kumar², Bin Guan³, Forrest M. Hoffman²

¹The University of Tennessee

²Oak Ridge National Laboratory

³University of California, Los Angeles

Key Points:

- Atmospheric Rivers (ARs) generally lead to a week-long persistent increase in daily temperature over Interior Alaska (AK)
- In AK, ARs account for 36% of total precipitation, 57% of extreme precipitation and explain 48% of interannual variability of precipitation
- AR events during the coldest months prolong the annual breakup date of river ice, while ARs closer to the breakup date have less impact.

14 **Abstract**

15 Atmospheric rivers (ARs) transport vast amounts of moisture from low to high lat-
 16 itude regions. One region particularly impacted by ARs is Interior Alaska (AK). We
 17 analyze the impact of ARs on the annual river ice breakup date for 25 locations in AK. We
 18 investigate the AR-driven rise in local temperatures and explore the relationship between
 19 ARs and precipitation, including extremes and interannual variability. We found that
 20 the increase in local temperatures after an AR event can last for as long as one week.
 21 Our results show that ARs account for 36% of total precipitation, explain 48% of pre-
 22 cipitation variability, and make up 57% of extreme precipitation events. Calculating the
 23 heat transfer between ARs and river ice, we conclude that heavy precipitation events (HPEs)
 24 during the coldest period of the year prolong river ice breakup dates, while HPEs occur-
 25 ring close to the breakup date have little impact on breakup timing.

26 **Plain language summary**

27 Atmospheric Rivers (ARs) are large storm systems originating in tropical regions
 28 capable of depositing large amounts of precipitation as far north as the Arctic. Using
 29 river ice breakup data recorded throughout Interior Alaska (AK) we set out to find whether
 30 there exists a link between ARs and annual river ice breakup timing. We determined that
 31 daily temperature increases can last up to one week after an AR event. We also found
 32 that ARs account for 36% of total annual precipitation from 1980 to 2023, explain 48%
 33 of the variability of precipitation, and make up 57% of extreme precipitation events. We
 34 then calculated the total heat transfer between precipitation and river ice and found that
 35 heavy precipitation events (HPEs), from both local precipitation and ARs, that occur
 36 relatively close to river ice breakup dates, have little correlation to the breakup date. How-
 37 ever, HPEs that occur during the coldest period of the year (typically late December to
 38 early-February) are strongly inversely correlated with river ice breakup timing, and there-
 39 fore prolong the breakup date.

40 **1 Introduction**

41 Atmospheric rivers (ARs) are narrow corridors of intense water vapor transport that
 42 significantly influence hydrologic events, transporting most of the water vapor outside
 43 of the Tropics (USDOC, 2023). It is estimated that ARs are responsible for as much as
 44 90% of poleward water vapor transport at midlatitudes (Zhu & Newell, 1998). ARs con-
 45 tribute to extreme precipitation events across various regions worldwide (Espinoza et al.,
 46 2018; Massoud et al., 2019), including Western North America (Dettinger et al., 2004;
 47 Neiman et al., 2008; Guan et al., 2010; Paul J. et al., 2011; Ralph et al., 2006; F. Mar-
 48 tin et al., 2019; Dettinger et al., 2011) Europe (Lavers et al., 2013; Harald & Andreas,
 49 2013), the Middle East (Massoud et al., 2020; Lashkari & Esfandiari, 2020; Esfandiari
 50 & Shakiba, 2024), and Western South America (Viale et al., 2018). In recent years, the
 51 impacts of ARs on the cryosphere such as Greenland (Mattingly et al., 2018) and Antarc-
 52 tica (Gorodetskaya et al., 2014; Wille et al., 2021), have been more extensively analyzed.

53 In recent years, a growing number of works investigating the relationship between
 54 ARs and high latitude regions has been underway. Evidence shows that between 1981
 55 and 2020, higher atmospheric moisture content was significantly correlated with lower
 56 sea ice coverage over almost the entire Arctic Ocean (Li et al., 2022). For those same years,
 57 another analysis found that 100% of extreme temperature events in the Arctic (above
 58 0 °C) coincide with the presence of ARs (Ma et al., 2023). Analyses have noted a rela-
 59 tionship between heavy AR activity and sea ice loss, caused by increased rainfall from
 60 moisture originating in lower latitudes (Zhang et al., 2023; MacLennan et al., 2022). How-
 61 ever Arctic systems are complicated, as the intense moisture transport within ARs can
 62 also result in heavy snowfall events, thus contributing to the accumulation of snowpack,

especially in mountainous regions (Saavedra et al., 2020; Guan et al., 2010). Under the right conditions, this relationship has been found to actually increase the mass balance of glaciers (Little et al., 2019). Understanding the role of ARs in the cryosphere is essential for assessing their broader impact on regional water resources and glacier dynamics in a changing climate.

While a number of works have explored the relationship between ARs and sea ice, glaciers, or ice sheets, to our knowledge there has been no analysis that investigates the relationship between ARs and Arctic river ice. Many works have used physics based processes to model the annual breakup timing and conditions of Arctic river ice (Paily et al., 1974; Ashton, 1986; T. Prowse et al., 2007; Jasek, 1998; Shen, 2010). Through such studies, it is recognized that an increase in precipitation leading to an increase in streamflow alters the hydraulics surrounding river ice breakup timing, potentially accelerating mechanical breakup events (Ashton, 1986). It has also been proposed that increased snow pack as a result of increased precipitation, contributes to breakup severity (T. D. Prowse & Beltoos, 2002). Using breakup records throughout Interior Alaska (AK) from the Alaska Pacific River Forecast Center Database (the same breakup records used in this analysis) Bieniek et al. (2011) determined that winter precipitation plays a relatively minor role in impacting the breakup timing of river ice and if anything accelerates the breakup timing as a result of increased streamflow. They go on to say that increased storm activity in the spring leads to increased surface air temperature, leading to earlier breakup dates (Bieniek et al., 2011). However, their analysis used only 4 sites (as opposed to the 25 used in this analysis) and aggregated precipitation seasonally without accounting for the interaction between winter precipitation and temperature that occurs at a finer temporal resolution.

Our analysis sets out to answer the following questions: 1.) Since ARs have been known to impact Arctic systems by increasing temperatures, is there a change in air temperature in different regions of AK corresponding to the presence of ARs? 2.) How do ARs contribute to precipitation throughout AK, considering how ARs impact total annual precipitation, interannual variability, and extreme events? 3.) How do ARs impact the timing of river ice breakup, does the presence of ARs accelerate or prolong the timing of river ice breakup?

2 Data

2.1 AR Catalog

Similar to previous studies, we define ARs using integrated vapor transport (IVT) values constructed from 6-hourly values of 3-D wind and water vapor at eight pressure levels between 300 and 1,000 mb from the National Center for Environmental Protection (NCEP) reanalysis data product (Kalnay et al., 1996). AR detection is based on version3 of the tARget algorithm (Guan & Waliser, 2019; Guan, 2022). The IVT values are calculated at the original resolution from the NCEP meteorological inputs (Saha et al., 2010). Guan and Waliser (2015) developed a global AR detection algorithm, which was updated and validated later with in situ and dropsonde data (Guan, 2022). This algorithm is employed for our study, which is based on a combination of the IVT magnitude, direction, and geometry characteristics, to objectively identify ARs. Contiguous regions of enhanced IVT transport are first identified from magnitude thresholding (i.e., grid cells with IVT above the seasonally and locally dependent 85th percentile, or $100 \frac{kg}{m*s}$, whichever is greater) and further filtered using directional and geometry criteria requirements. Although the $100 \frac{kg}{m*s}$ threshold is applied globally, it is intended for dry (including polar) regions since in other regions the 85th percentile is already larger than $100 \frac{kg}{m*s}$. The detection algorithm was applied to NCEP in its native resolution of 2.5° . This detection algorithm had over 90% agreement in detecting AR landfall dates when compared

113 with other AR detection methods, for Western North America (Neiman et al., 2008), the
 114 United Kingdom (Lavers et al., 2011), and East Antarctica (Gorodetskaya et al., 2014).

115 2.2 Daymet Daily Surface Weather and Climatological Summaries

116 Precipitation and daily minimum and maximum temperatures (T_{\min} and T_{\max} re-
 117 spectively) from Oak Ridge National Laboratory's Daymet $1km \times 1km$ daily product were
 118 used, via the Distributed Active Archive Center (M. Thornton et al., 2022). Daymet pre-
 119 cipitation, T_{\min} and T_{\max} , were used in our analysis as they have a strong agreement with
 120 NCEP temperature outputs for our region of interest Figure 1C. Additionally, because
 121 Daymet is derived directly from in situ instruments and meteorological stations, it rep-
 122 presents a robust dataset for precipitation and temperature predictions across North Amer-
 123 ica (P. E. Thornton et al., 2021). This dataset has been a standard for validation among
 124 several analyses related to arctic regions (Diro & Sushama, 2019; Akinsanola et al., 2024).
 125 The annual mean precipitation and temperature for the year 2021 over the AK region
 126 are shown in Figure 1AB, and Figure 1C shows the temperature profiles, precipitation
 127 and AR trends for one of those location over one year (Crooked Creek at the Kuskok-
 128 wim River in 2021).

129 2.3 River ice breakup records

130 River ice breakup dates were obtained from the Alaska Pacific River Forecast Cen-
 131 ter database. While exact coordinates were unavailable, locations were estimated based
 132 on proximity to weather stations and airports, to maintain spatial consistency with in-
 133 puts used in Daymet's meteorological models. There were 25 locations (shown in Fig-
 134 ure 1) identified as having at least 35 breakup records between 1980 and 2023 (the cur-
 135 rent temporal availability of Daymet), although breakup records go as far back as 1896
 136 for some locations. The 35 breakup records threshold was used because it allowed for
 137 the greatest number of locations with the most complete time series necessary for sta-
 138 tistical analysis. There is always one breakup date per year, but not every year has a
 139 recorded date, so some years are represented as empty values in the dataset. On aver-
 140 age, recorded break up dates range from mid March to late June. This dataset has been
 141 used in other analyses such as (Murphy et al., 2022; Brown et al., 2018; Bieniek et al.,
 142 2011). As an example, the breakup date for Crooked Creek at the Kuskokwim River in
 143 2021 occurred in early May and is depicted in Figure 1C with a vertical purple dashed
 144 line.

145 3 Methods

146 To assess the influence of ARs on local temperature, we analyze the relationship
 147 between the presence of an AR and the temperature change at a specific location. The
 148 presence of an AR is represented numerically as a binary value indicating whether or not
 149 an AR is active on a particular date. We then estimate how many days this change in
 150 temperature lasts. To do this, we used a varying temporal window combined with a pair-
 151 wise t-test. In other words, for each AR occurrence in the dataset, a lookback window
 152 and forecast window each equal to n days in length was created before and after the AR
 153 date, respectively, whereby: $n \in \{1, 2, 3, \dots, 14\}$. For values of n greater than one day
 154 the mean was taken within each window for T_{\min} and T_{\max} . These aggregated temper-
 155 atures were then calculated over all locations. Aggregated temperature pairs were as-
 156 sessed using a one tailed pairwise t-test to check whether ARs increased the local tem-
 157 perature over period of time n ($\alpha = 0.05$).

158 We then explored how ARs contribute to precipitation, by separating AR-based
 159 precipitation from the total amount. We then used the Wilcoxon rank-sum test (Rey &
 160 Neuhauser, 2011) to test the hypothesis that AR events tend to produce more precip-

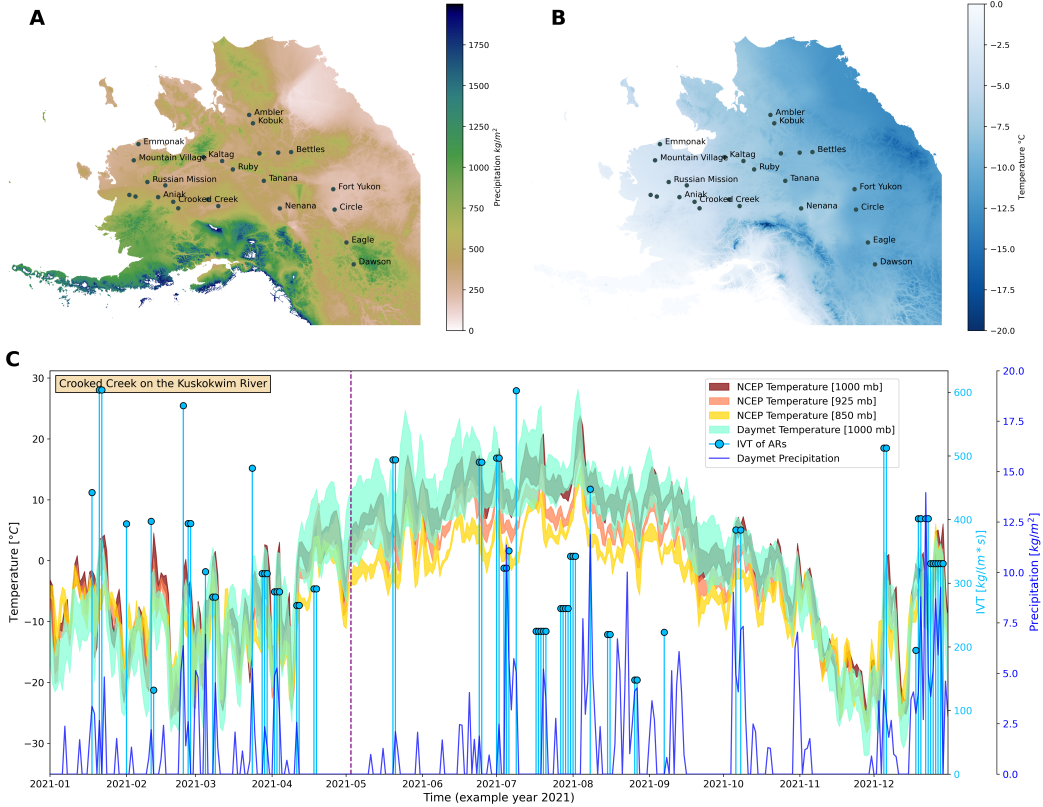


Figure 1. top row: (left) map showing summated precipitation for the year 2021; (right) map of average temperature for 2021. bottom row: One of the 25 locations (Crooked Creek on the Kuskokwim River) for the year 2021. Yellow, orange, red represent the temperature profiles (fill plot of $T_{\min} - T_{\max}$) from NCEP temperature data at 850, 925 and 1000mb respectively. Light green represents the Daymet temperature profile. Dark blue shows modeled precipitation from Daymet ($\frac{\text{kg}}{\text{m} \cdot \text{s}^2}$) relative to the y-axis in dark blue on the right. The light blue stem plots depict the IVT of AR events ($\frac{\text{kg}}{\text{m} \cdot \text{s}}$) relative to the y-axis in light blue on the right. The vertical purple dashed line shows the breakup date for the Kuskokwim River in 2021 for Crooked Creek.

161 iteration than other precipitation events. We opted to use a non-parametric test (Wilcoxon
 162 rank-sum test) because the distributions of precipitation were shown to not be normally
 163 distributed after log transformation using the Shapiro-Wilks test, (Shapiro & Wilk, 1965).
 164 We also estimated the interannual variability of precipitation that ARs account for by
 165 conducting a univariate ordinary least squares regression (OLS). For extremes, we ex-
 166 tracted the top 5% of precipitation events and determined what fraction of those events
 167 are associated with ARs.

168 To determine the impact that ARs have on river ice breakup timing, we used in-
 169 formation on heat transfer estimated using Equation 1:

$$\frac{dQ}{dt} = \rho \cdot m \cdot \Delta T \quad (1)$$

170 where Q is heat flux ($\frac{J}{m^2}$); ρ specific heat ($\frac{J}{g \cdot ^\circ C}$); ΔT is the difference of ambient tem-
 171 perature and the river ice surface (which is estimated using T_{min} as a proxy for ambi-
 172 ent) ($^\circ C$); m the mass of the precipitation (kg). The integral of these values over all pre-
 173 precipitation events that occurred six months prior to the breakup date is taken with re-
 174 spect to time. A temporal bias function (Equation 2) with tunable parameters is applied
 175 to the heat transfer equation to assess the days of the year in which precipitation events
 176 were more impactful on breakup timing:

$$f(t; \gamma, \kappa, DOY, c) = \begin{cases} \frac{e^{-\gamma \cdot (-t - DOY)} - 1}{e^{-\gamma \cdot (t - DOY)} - 1} & \text{if } t < c \\ \frac{\kappa}{e^{-\gamma \cdot (t - DOY)} - 1} & \text{if } t \geq c \end{cases} \quad (2)$$

177 where γ is a tunable parameter impacting the width of the exponential function; t is time
 178 in days; DOY is the Gregorian day of year that the breakup date occurred; c is a tun-
 179 able parameter dictating the center placement of the function; κ is a normalizing con-
 180 stant. Finally, Equation 3 is tuned over the entire hyperparameter search space for each
 181 location, optimized by selecting the parameter values that produce the Pearson corre-
 182 lation coefficient with the greatest absolute value.

$$\int_{t_i}^{t_{DOY}} \left(f(t; \gamma, \kappa, DOY, c) \cdot \frac{dQ}{dt} \right) dt \quad (3)$$

183 4 Results

184 4.1 AR impact on temperature

185 We applied the pairwise t-test comparing lookback and forecast windows of length
 186 n . Figure 2 shows the change in p-values for each value of n (top row) as well as the mean
 187 increase in temperature from the lookback window to the forecast window (bottom row).
 188 The mean temperature increase tends to be higher for T_{min} post AR than T_{max} , with
 189 both plots showing a clear downward trend as the length of n increases. We found that
 190 there is a statistically significant difference in T_{min} (based on an $\alpha = 0.05$) roughly 8
 191 days before and after an AR event. This was true for all locations in the study as rep-
 192 resented by the fill plot (Figure 2A). This increase in temperature can be as high as 1.5
 193 $^\circ C$ ($n = 2$) (Figure 2C). The t-test for T_{max} implies that the presence of an AR can in-
 194 crease temperatures for roughly 6 days on average (Figure 2B), with an increase as high
 195 as 0.75 $^\circ C$ ($n = 3, 4$) (Figure 2D).

196 4.2 AR impact on precipitation

197 Figure 3 shows the AR-based IVT (Figure 3A) and total precipitation (Figure 3B)
 198 through the span of the data record, spatially aggregated over all locations. ARs tend

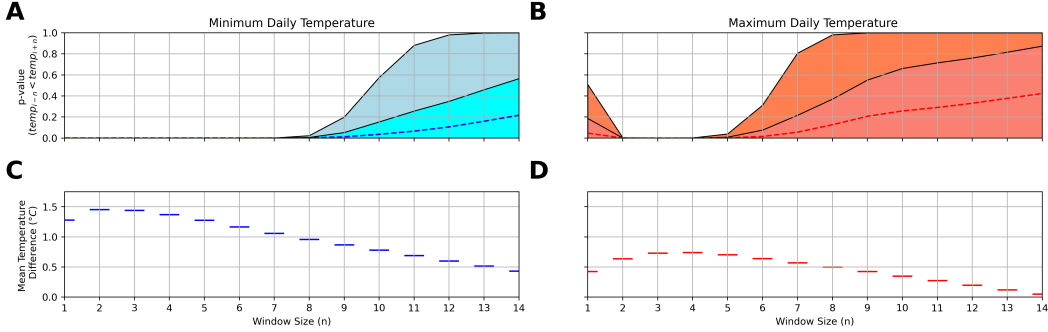


Figure 2. top row: the p-values of the paired t-test given the window size (n) surrounding the AR event date (left: T_{\min} ; right: T_{\max}). Dashed lines represent the mean p-value over the study area. For example, looking at T_{\min} on the left, the light blue represents the 25th to the 75th percentile or IQR of p-values, while the blue-grey is the 75th percentile to the maximum p-value given n . Same is true for the color transition of T_{\max} . bottom row: the average increase in temperature based on AR events, calculated from the lookback window to the forecast window.

to account for 36% of precipitation on average (Figure 3C), with a high degree of variability given the year and location. In 2005 and 2020, for example, ARs accounted for nearly 80% of the total precipitation in some locations. Furthermore, the results from the Wilcoxon rank-sum test show that precipitation from ARs tends to be greater in magnitude than non-AR precipitation (test statistic = -83.85 ; p-value ≈ 0.0). In addition, it was found that of the top 5% of high precipitation events (HPEs), 57% were caused by ARs (Figure 4A). Correlating annual aggregated precipitation from ARs, to total annual aggregated precipitation in a univariate OLS, we find that the coefficient of variation (R^2) is equal to 0.48 (Figure 4B). This indicates that ARs explain about 48% of interannual variability in precipitation, over all 25 locations.

4.3 Transfer of energy based on Precipitation

To estimate the impact HPEs have on river ice breakup dates, we use Equation 3 to calculate the heat transfer between precipitation and the river ice surface. In essence, this exercise allows us to take the energy input from precipitation (whether AR-based or not) and determine whether or not that integrated energy accelerates or decelerates the breakup of river ice. We find that there is a strong negative correlation between the heat transfer and the DOY in which the river ice breaks (Figure 5A). In this context, negative values along the y-axis of Figures 5A and 5D are interpreted as a negative heat exchange, meaning a cooling effect on the river ice surface or a deposition of precipitation below freezing. This is optimized for when the temporally-weighted bias curve is positioned during the coldest period of the year - typically between late November and early February (Figure 5C). Table 1 shows the correlation for each location, after tuning parameters c and γ are applied to Equation 3. Table 1 also shows the center of the bias curve c (month-day) that was selected for at each location, given the integrand for precipitation used in Equation 3 (ie. Total Precipitation, Precipitation from ARs, Precipitation not from ARs). For example, Crooked Creek on the Kuskokwim River has a clear negative trend, with HPE causing a cooling effect on the river ice surface, prolonging the DOY. This relationship has a Pearson correlation coefficient (r_p) = -0.84 and a Spearman correlation coefficient (r_s) = -0.80 , indicating that HPEs of greater magnitude, occurring during the coldest period of the year, lead to a delaying of the breakup date. The relationship between the total number of ARs that occurred six months prior

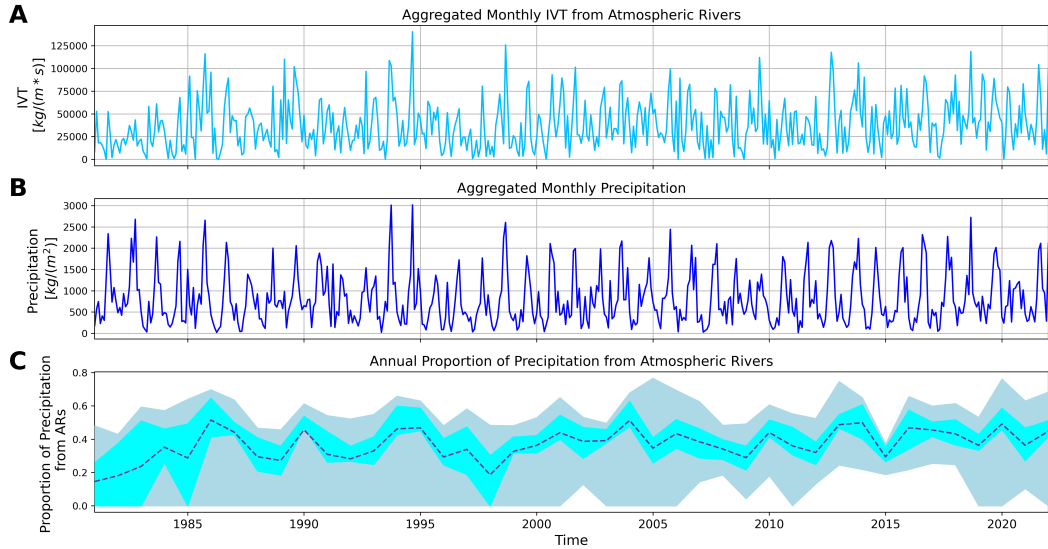


Figure 3. top row: time series of IVT $\frac{\text{kg}}{\text{m} * \text{s}}$ aggregated monthly over all locations. middle row: time series of total precipitation $\frac{\text{kg}}{\text{m}^2}$ aggregated monthly over all locations. bottom row: proportion of precipitation accounted for by ARs on an annual basis. Light blue depicts the 25th to 75th percentile (IQR) of proportion values, while the blue-grey represents proportions outside of the IQR, over all 25 locations. The dashed line represents the mean proportion.

230 to the breakup date and the DOY are shown in the center column (Figure 5B and 5E;
 231 these two plots are the same by definition) indicating that the number of AR events that
 232 occur within the six months prior to the breakup is insufficient information in correlat-
 233 ing to breakup timing on its own. The bottom row of Figure 5 shows that the use of a
 234 bias function (Equation 2) is necessary, as simply applying the integral of Equation 1
 235 using an equally weighted temporal bias function (the aggregated total heat transfer)
 236 is uncorrelated.

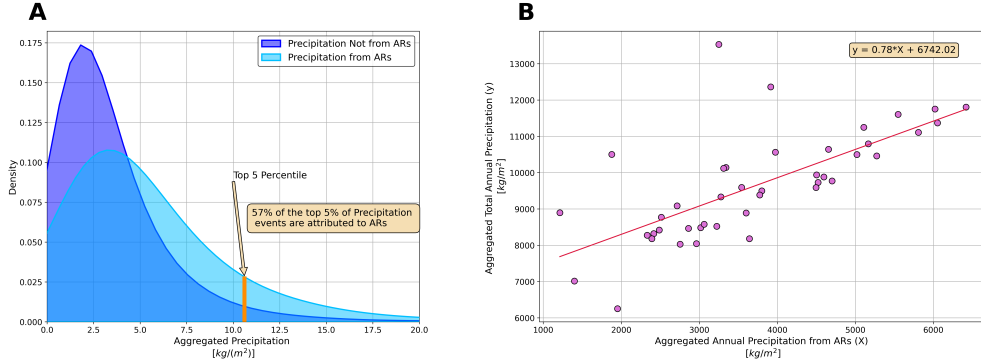


Figure 4. left: kernel density plots showing the distribution of local precipitation (dark blue) and precipitation from ARs (light blue). right: ordinary least squares regression plot using annual, summated precipitation from ARs, to predict total annual summed precipitation.

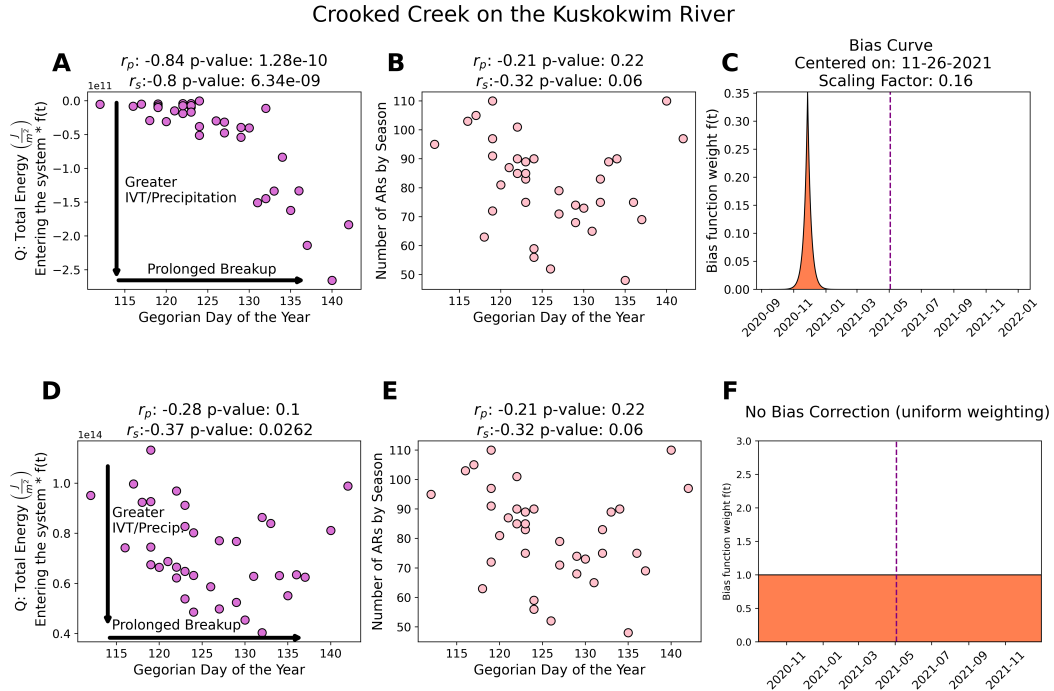


Figure 5. top: (left) scatter plot between thermal energy transfer and DOY (the Gregorian day of year that the breakup date occurred); (middle) scatter plot of the number of ARs that occurred in the six months prior to the breakup date and DOY; (right) temporal bias curve for the year 2021 with the breakup date represented by the vertical dashed line. bottom: same as the top except depicting the results when a temporal bias is not utilized.

237 5 Conclusion and Discussion

238 This study investigated the impact atmospheric rivers (ARs) and heavy precipi-
 239 tation events (HPEs) have on the breakup dates of river ice in Alaska. We explored the
 240 relationship of ARs to temperature increases throughout the study domain, the contri-

241 bution of ARs to various precipitation metrics, including variability and extremes, and
 242 determined the impact of ARs and HPEs on the DOY in which the ice on the surface
 243 of Alaskan rivers eventually breaks.

244 For temperature increases, we found that ARs generally lead to a week-long per-
 245 sistent increase in daily temperature over Alaska, with temperatures rising by as much
 246 as 1.5°C for T_{\min} and 0.75°C for T_{\max} . This result makes sense, as noted by many past
 247 works showing how warm moisture brought on by ARs can warm the cryosphere (Wille
 248 et al., 2021; Ma et al., 2023; Li et al., 2022; Zhang et al., 2023). For the contribution to
 249 precipitation, our results show that ARs account for a significant portion of precipita-
 250 tion in Alaska, contributing to 36% of total precipitation on average. They also explain
 251 48% of interannual variability and make up 57% of extreme precipitation events (pre-
 252 precipitation events within the top 5% of deposition). As for the relationship between ARs
 253 and river ice breakup, we show evidence that intense ARs occurring during the coldest
 254 period of the year appear to prolong the annual breakup date of river ice. Our results
 255 do not show that ARs are unique relative to local forms of precipitation in this regard
 256 (Table 1) with no evidence that increased precipitation events of any kind closer to the
 257 breakup date accelerates the breakup date. This is likely attributed to a combination
 258 of the heat transfer from precipitation, as well as changes in the river ice surface as a re-
 259 sult of snowfall. Increased snow coverage will increase the albedo of the river surface,
 260 as well as insulate it, mitigating temperature fluctuations during the coldest period of
 261 the year.

262 Overall, understanding the role of ARs and other HPEs in the timing of river ice
 263 break up in Alaska is crucial for predicting and managing the impacts of climate change
 264 in the region, especially since studies have shown that AR frequency and intensity in this
 265 region are expected to increase in a warmer world (Espinoza et al., 2018; Massoud et al.,
 266 2019). The findings suggest that ARs contribute significantly to the hydrology and cli-
 267 mate of Alaska, affecting temperature, precipitation, and river ice dynamics. Further re-
 268 search in this area could help improve our understanding of ARs and their role in shap-
 269 ing the climate of high-latitude regions.

270 Data Availability Statement

271 Daily Daymet precipitation and temperature data is available through the Oak Ridge
 272 National Laboratory Distributed Active Archive at [https://daymet.ornl.gov/single](https://daymet.ornl.gov/single-pixel/)
 273 [-pixel/](https://daymet.ornl.gov/single-pixel/). The National Center for Environmental Protection temperature data can be found
 274 at <https://psl.noaa.gov/data/index.html>. River ice breakup records are maintained
 275 by the Alaska Pacific River Forecast Center at <https://www.weather.gov/aprfc/breakupMap>.
 276 The Global Atmospheric River database is maintained by the UCLA Dataverse and can
 277 be accessed at [https://dataverse.ucla.edu/dataset.xhtml?persistentId=doi:10](https://dataverse.ucla.edu/dataset.xhtml?persistentId=doi:10.25346/S6/Y015ON)
 278 .25346/S6/Y015ON.

279 Acknowledgments

280 The AR database (<https://doi.org/10.25346/S6/Y015ON>) was provided by Bin Guan
 281 via the Global Atmospheric Rivers Dataverse (<https://dataverse.ucla.edu/dataverse/ar>).
 282 Development of the AR database was supported by NASA and the California Depart-
 283 ment of Water Resources.

284 References

- 285 Akinsanola, A. A., Jung, C., Wang, J., & Kotamarthi, V. R. (2024). Evaluation
 286 of precipitation across the contiguous united states, alaska, and puerto rico in
 287 multi-decadal convection-permitting simulations. *Scientific Reports*, 14(1),
 288 1238. Retrieved from <https://doi.org/10.1038/s41598-024-51714-3> doi:

- 289 10.1038/s41598-024-51714-3
- 290 Ashton, G. (1986). *River and lake ice engineering*. Water Resources Publications.
- 291 Retrieved from <https://books.google.com/books?id=xg1YVjAsnt8C>
- 292 Bieniek, P. A., Bhatt, U. S., Rundquist, L. A., Lindsey, S. D., Zhang, X., &
- 293 Thoman, R. L. (2011). Large-scale climate controls of interior alaska river
- 294 ice breakup. *Journal of Climate*, 24(1), 286 - 297. Retrieved from <https://journals.ametsoc.org/view/journals/clim/24/1/2010jcli3809.1.xml>
- 295 doi: 10.1175/2010JCLI3809.1
- 296 Brown, D. R. N., Brinkman, T. J., Verbyla, D. L., Brown, C. L., Cold, H. S., &
- 297 Hollingsworth, T. N. (2018). Changing river ice seasonality and impacts on
- 298 interior alaskan communities. *Weather, Climate, and Society*, 10(4), 625 - 640.
- 299 Retrieved from https://journals.ametsoc.org/view/journals/wcas/10/4/wcas-d-17-0101_1.xml doi: 10.1175/WCAS-D-17-0101.1
- 300 Dettinger, M. D., Cayan, D. R., Meyer, M. K., & Jeton, A. E. (2004). Simulated
- 301 hydrologic responses to climate variations and change in the merced, carson,
- 302 and american river basins, sierra nevada, california, 1900–2099. *Climatic*
- 303 *Change*, 62(1), 283–317. Retrieved from <https://doi.org/10.1023/B:CLIM.0000013683.13346.4f>
- 304 Dettinger, M. D., Ralph, F. M., Das, T., Neiman, P. J., & Cayan, D. R. (2011).
- 305 Atmospheric rivers, floods and the water resources of california. *Water*, 3(2),
- 306 445–478. Retrieved from <https://www.mdpi.com/2073-4441/3/2/445> doi:
- 307 10.3390/w3020445
- 308 Diro, G. T., & Sushama, L. (2019). Simulating canadian arctic climate at
- 309 convection-permitting resolution. *Atmosphere*, 10(8). Retrieved from
- 310 <https://www.mdpi.com/2073-4433/10/8/430> doi: 10.3390/atmos10080430
- 311 Esfandiari, N., & Shakiba, A. (2024). The extraordinary atmospheric rivers
- 312 analysis over the middle east: Large-scale drivers, structure, effective
- 313 sources, and precipitation characterization. *Dynamics of Atmospheres and*
- 314 *Oceans*, 105, 101430. Retrieved from <https://www.sciencedirect.com/science/article/pii/S0377026523000817> doi: <https://doi.org/10.1016/j.dynatmoce.2023.101430>
- 315 Espinoza, V., Waliser, D. E., Guan, B., Lavers, D. A., & Ralph, F. M. (2018).
- 316 Global analysis of climate change projection effects on atmospheric rivers.
- 317 *Geophysical Research Letters*, 45(9), 4299-4308. Retrieved from <https://agupubs.onlinelibrary.wiley.com/doi/abs/10.1029/2017GL076968> doi:
- 318 <https://doi.org/10.1029/2017GL076968>
- 319 F. Martin, R., Jonathan J., R., Jason M., C., Michael, D., Michael, A., David, R.,
- 320 ... Chris, S. (2019). A scale to characterize the strength and impacts of atmo-
- 321 spheric rivers. *Bulletin of the American Meteorological Society*, 100(2), 269 -
- 322 289. Retrieved from <https://journals.ametsoc.org/view/journals/bams/100/2/bams-d-18-0023.1.xml> doi: 10.1175/BAMS-D-18-0023.1
- 323 Gorodetskaya, I. V., Tsukernik, M., Claes, K., Ralph, M. F., Neff, W. D., &
- 324 Van Lipzig, N. P. M. (2014). The role of atmospheric rivers in anomalous snow
- 325 accumulation in east antarctica. *Geophysical Research Letters*, 41(17), 6199-
- 326 6206. Retrieved from <https://agupubs.onlinelibrary.wiley.com/doi/abs/10.1002/2014GL060881> doi: <https://doi.org/10.1002/2014GL060881>
- 327 Guan, B. (2022). [Data] *Global Atmospheric Rivers Database, Version 3*. UCLA
- 328 Dataverse. Retrieved from <https://doi.org/10.25346/S6/Y0150N> doi: 10
- 329 .25346/S6/Y0150N
- 330 Guan, B., Molotch, N. P., Waliser, D. E., Fetzer, E. J., & Neiman, P. J. (2010).
- 331 Extreme snowfall events linked to atmospheric rivers and surface air tem-
- 332 perature via satellite measurements. *Geophysical Research Letters*, 37(20).
- 333 Retrieved from <https://agupubs.onlinelibrary.wiley.com/doi/abs/10.1029/2010GL044696> doi: <https://doi.org/10.1029/2010GL044696>
- 334 Guan, B., & Waliser, D. (2019, 12). Tracking atmospheric rivers globally: Spa-

- 344 tial distributions and temporal evolution of life cycle characteristics. *Journal of*
 345 *Geophysical Research: Atmospheres*, 124. doi: 10.1029/2019JD031205
- 346 Guan, B., & Waliser, D. E. (2015). Detection of atmospheric rivers: Evaluation
 347 and application of an algorithm for global studies. *Journal of Geophysical Re-*
 348 *search: Atmospheres*, 120(24), 12514-12535. Retrieved from <https://agupubs.onlinelibrary.wiley.com/doi/abs/10.1002/2015JD024257> doi: <https://doi.org/10.1002/2015JD024257>
- 351 Harald, S., & Andreas, S. (2013). Moisture origin and meridional trans-
 352 port in atmospheric rivers and their association with multiple cyclones.
 353 *Monthly Weather Review*, 141(8), 2850 - 2868. Retrieved from <https://journals.ametsoc.org/view/journals/mwre/141/8/mwr-d-12-00256.1.xml>
 354 doi: 10.1175/MWR-D-12-00256.1
- 355 Jasek, M. (1998, July 27–31). 1998 break-up and flood on the yukon river at dawson
 356 – did el niño and climate change play a role? In H. Shen (Ed.), *Ice in surface*
 357 *waters: Proceedings of the 14th international symposium on ice* (pp. 761–768).
 358 Rotterdam: A.A. Balkema.
- 360 Kalnay, E., Kanamitsu, M., Kistler, R., Collins, W., Deaven, D., Gandin, L., ...
 361 Joseph, D. (1996). The ncep/ncar 40-year reanalysis project. *Bulletin*
 362 *of the American Meteorological Society*, 77(3), 437 - 472. Retrieved from
 363 https://journals.ametsoc.org/view/journals/bams/77/3/1520-0477_1996_077_0437_tnyrp_2.0.co_2.xml doi: 10.1175/1520-0477(1996)077<0437:TNYRP>2.0.CO;2
- 366 Lashkari, H., & Esfandiari, N. (2020, 05). Identifying atmospheric river events and
 367 their paths into iran. *Theoretical and Applied Climatology*, 140. doi: 10.1007/
 368 s00704-020-03148-w
- 369 Lavers, D. A., Allan, R. P., Villarini, G., Lloyd-Hughes, B., Brayshaw, D. J., &
 370 Wade, A. J. (2013). Future changes in atmospheric rivers and their impli-
 371 cations for winter flooding in britain. *Environmental Research Letters*, 8(3).
 372 Retrieved from <https://doi.org/10.1088/1748-9326/8/3/034010> doi:
 373 10.1088/1748-9326/8/3/034010
- 374 Lavers, D. A., Allan, R. P., Wood, E. F., Villarini, G., Brayshaw, D. J., & Wade,
 375 A. J. (2011). Winter floods in britain are connected to atmospheric
 376 rivers. *Geophysical Research Letters*, 38(23). Retrieved from <https://agupubs.onlinelibrary.wiley.com/doi/abs/10.1029/2011GL049783> doi:
 377 <https://doi.org/10.1029/2011GL049783>
- 379 Li, L., Cannon, F., Mazloff, M. R., Subramanian, A. C., Wilson, A. M., & Ralph,
 380 F. M. (2022). Impact of atmospheric rivers on arctic sea ice variations. *EGU-*
 381 *sphere*, 2022, 1–21. Retrieved from <https://egusphere.copernicus.org/preprints/2022/egusphere-2022-36/> doi: 10.5194/egusphere-2022-36
- 383 Little, K., Kingston, D. G., Cullen, N. J., & Gibson, P. B. (2019). The role of at-
 384 mospheric rivers for extreme ablation and snowfall events in the southern alps
 385 of new zealand. *Geophysical Research Letters*, 46(5), 2761-2771. Retrieved
 386 from <https://agupubs.onlinelibrary.wiley.com/doi/abs/10.1029/2018GL081669> doi: <https://doi.org/10.1029/2018GL081669>
- 388 Ma, W., Wang, H., Chen, G., Qian, Y., Baxter, I., Huo, Y., & Seefeldt, M. W.
 389 (2023). Wintertime extreme warming events in the high arctic: Characteristics,
 390 drivers, trends, and the role of atmospheric rivers. *EGUsphere*. Retrieved
 391 from <https://doi.org/10.5194/egusphere-2023-2018> (Preprint) doi:
 392 10.5194/egusphere-2023-2018
- 393 Maclennan, M. L., Lenaerts, J. T. M., Shields, C., & Wille, J. D. (2022). Contri-
 394 bution of atmospheric rivers to antarctic precipitation. *Geophysical Research*
 395 *Letters*, 49(18). Retrieved 2024-04-16, from <https://onlinelibrary.wiley.com/doi/abs/10.1029/2022GL100585> doi: 10.1029/2022GL100585
- 397 Massoud, E., Espinoza, V., Guan, B., & Waliser, D. (2019). Global cli-
 398 mate model ensemble approaches for future projections of atmospheric

- 454 doi: 10.1175/2010BAMS3001.1
- 455 Shapiro, S. S., & Wilk, M. B. (1965). An analysis of variance test for normality
 456 (complete samples). *Biometrika*, 52(3-4), 591–611.
- 457 Shen, H. T. (2010). Mathematical modeling of river ice processes. *Cold Re-
 458 gions Science and Technology*, 62(1), 3-13. Retrieved from <https://www.sciencedirect.com/science/article/pii/S0165232X10000339> doi:
 459 <https://doi.org/10.1016/j.coldregions.2010.02.007>
- 460 Thornton, M., Shrestha, R., Wei, Y., Thornton, P., Kao, S.-C., & Wilson, B.
 461 (2022). *Daymet: Annual climate summaries on a 1-km grid for north america,
 462 version 4 r1*. ORNL Distributed Active Archive Center. Retrieved
 463 from https://daac.ornl.gov/cgi-bin/dsviewer.pl?ds_id=2130 doi:
 464 <https://doi.org/10.3334/ORNLDAAAC/2130>
- 465 Thornton, P. E., Shrestha, R., Thornton, M., Kao, S.-C., Wei, Y., & Wilson,
 466 B. E. (2021, 7 23). Gridded daily weather data for north america with
 467 comprehensive uncertainty quantification. *Scientific Data*, 8(1), 190. Re-
 468 trieval from <https://doi.org/10.1038/s41597-021-00973-0> doi:
 469 [10.1038/s41597-021-00973-0](https://doi.org/10.1038/s41597-021-00973-0)
- 470 USDOC. (2023, 3). *What are atmospheric rivers?* National Oceanic and At-
 471 mospheric Administration. Retrieved from [https://www.noaa.gov/stories/
 473 what-are-atmospheric-rivers](https://www.noaa.gov/stories/

 472 what-are-atmospheric-rivers)
- 474 Viale, M., Valenzuela, R., Garreaud, R. D., & Ralph, F. M. (2018). Impacts
 475 of atmospheric rivers on precipitation in southern south america. *Jour-
 476 nal of Hydrometeorology*, 19(10), 1671 - 1687. Retrieved from https://journals.ametsoc.org/view/journals/hydr/19/10/jhm-d-18-0006_1.xml
 477 doi: 10.1175/JHM-D-18-0006.1
- 478 Wille, J. D., Favier, V., Gorodetskaya, I. V., Agosta, C., Kittel, C., Beeman, J. C.,
 479 ... Codron, F. (2021). Antarctic atmospheric river climatology and pre-
 480 cipitation impacts. *Journal of Geophysical Research: Atmospheres*, 126(8),
 481 e2020JD033788. Retrieved from <https://agupubs.onlinelibrary.wiley.com/doi/abs/10.1029/2020JD033788> (e2020JD033788 2020JD033788) doi:
 482 <https://doi.org/10.1029/2020JD033788>
- 483 Zhang, P., Chen, G., Ting, M., Ruby Leung, L., Guan, B., & Li, L. (2023, March).
 484 More frequent atmospheric rivers slow the seasonal recovery of arctic sea ice.
 485 *Nature Climate Change*, 13(3), 266–273. Retrieved from <https://doi.org/10.1038/s41558-023-01599-3> doi: 10.1038/s41558-023-01599-3
- 486 Zhu, Y., & Newell, R. E. (1998). A proposed algorithm for moisture fluxes
 487 from atmospheric rivers. *Monthly Weather Review*, 126(3), 725 - 735.
 488 Retrieved from https://journals.ametsoc.org/view/journals/mwre/126/3/1520-0493_1998_126_0725_apafmf_2.0.co_2.xml doi: 10.1175/1520-0493(1998)126(0725:APAFMF)2.0.CO;2
- 489
- 490
- 491
- 492
- 493

494 **Appendix A.**

Table 1. Table showing the Pearson correlation coefficient with the optimal center placement of the temporal bias (month-day) by location [r_p /center date of bias]

Location	Total Precipitation	Precipitation from ARs	Precipitation not from ARs
Akiak Kuskokwim River	-0.78/11-12	-0.78/2-5	-0.8/1-15
Allakaket Koyukuk River	-0.81/12-10	-0.69/10-23	-0.8/12-3
Ambler Kobuk River	-0.84/2-5	-0.67/2-5	-0.83/2-12
Aniak Kuskokwim River	-0.8/11-19	-0.81/1-29	-0.77/11-12
Bethel Kuskokwim River	-0.72/12-3	-0.75/2-5	-0.73/12-10
Bettles Koyukuk River	-0.79/2-19	-0.7/10-23	-0.81/2-12
Circle Yukon River	-0.75/2-5	-0.76/1-22	-0.74/2-12
Crooked Creek Kuskokwim River	-0.84/11-26	-0.76/2-5	-0.8/11-26
Dawson Yukon River	-0.77/10-23	-0.67/1-22	-0.75/10-23
Eagle Yukon River	-0.77/10-23	-0.79/1-22	-0.76/1-29
Emmonak Yukon River	-0.76/2-5	-0.76/1-29	-0.71/4-16
Fort Yukon Yukon River	-0.72/10-23	-0.59/2-5	-0.72/10-23
Galena Yukon River	-0.79/11-19	-0.75/1-15	-0.8/4-16
Holy Cross Yukon River	-0.75/1-8	-0.77/1-8	-0.72/1-8
Hughes Koyukuk River	-0.81/1-1	-0.78/1-15	-0.78/4-2
Kaltag Yukon River	-0.84/12-3	-0.77/12-3	-0.86/1-15
Kobuk Kobuk River	-0.81/1-8	-0.62/4-16	-0.81/1-8
McGrath Kuskokwim River	-0.81/3-26	-0.81/2-5	-0.82/4-9
Mountain Village Yukon River	-0.72/1-29	-0.76/2-5	-0.69/2-19
Nenana Tanana River	-0.71/1-1	-0.73/2-5	-0.72/1-1
Nikolai Kuskokwim River	-0.75/2-12	-0.7/2-5	-0.74/1-15
Red Devil Kuskokwim River	-0.79/12-3	-0.8/2-5	-0.78/12-3
Ruby Yukon River	-0.83/4-9	-0.78/1-15	-0.86/4-16
Russian Mission Yukon River	-0.71/11-26	-0.72/12-10	-0.68/12-3
Tanana Yukon River	-0.76/1-22	-0.7/2-5	-0.77/11-26